

# Thermal Properties of Impurity-Doped Clusters: Orbital-Free Molecular Dynamics Simulations of the Meltinglike Transition in $\text{Li}_1\text{Na}_{54}$ and $\text{Cs}_1\text{Na}_{54}$

Andrés Aguado,\* Luis E. González, and José M. López

*Departamento de Física Teórica, Universidad de Valladolid, Valladolid 47011, Spain*

*Received: February 17, 2004; In Final Form: May 27, 2004*

The melting-like transition in  $\text{Li}_1\text{Na}_{54}$  and  $\text{Cs}_1\text{Na}_{54}$  clusters is studied by using constant-energy molecular dynamics simulations. An orbital-free density functional theory technique is used, which scales linearly with system size, allowing efficient investigation of thermal behavior in these medium-size clusters. The range of temperatures covered by our simulations is from 50 to 450 K, and the total simulation time (for each cluster) is about 1.50 ns. This simulation time allows the extraction of statistically meaningful values for the thermal averages of several melting indicators (specific heat, diffusion constants, etc). The ground-state isomer of both clusters is shown to be icosahedral, with the Li atom located at the center of the icosahedron and the Cs atom occupying a vertex surface position. Orbital-free predictions for relative stabilities and structures of different isomers are contrasted with corresponding Kohn–Sham calculations in order to judge the reliability of our approach. The results show that both clusters melt in several steps, each one related to the activation of diffusive motion in selected groups of atoms. Nevertheless, only one broad peak is observed in the thermal evolution of the specific heat. Melting temperatures  $T_m$ , as measured from the specific heat peaks (at approximately 110 and 130 K for  $\text{Cs}_1\text{Na}_{54}$  and  $\text{Li}_1\text{Na}_{54}$ , respectively), are different, suggesting the possibility of controlling the melting temperature of clusters by selective doping, and substantially lower than those of  $\text{Na}_{55}$ . Interesting differences in the melting behavior of both clusters, due to the size-mismatch effect, are highlighted. We also question the usual identification of melting temperature with the main peak in the thermal evolution of the specific heat. Several alternative definitions of melting temperature are then pursued. If we define, for example,  $T_m$  as the lowest temperature for which all atoms are able to diffuse across the whole cluster volume, very different values may be obtained.

## I. Introduction

Recent experimental and theoretical efforts have been devoted to obtain an understanding of the melting-like transition in finite clusters. This is important at both fundamental and applied levels: For example, the catalytic activity of small platinum clusters depends critically on their melting temperatures.<sup>1</sup> Also, the reduced number of atoms in small clusters causes new thermal processes to appear that are specific to this size regime and therefore not observed in macroscopic materials. By investigation of the temperature dependence of photofragmentation spectra, Haberland and co-workers<sup>2</sup> have deduced the melting temperatures of  $\text{Na}_N$  ( $N = 50\text{--}200$ ) clusters. A plot of the melting temperature as a function of cluster size shows local maxima for some sizes and a somewhat erratic behavior for the rest of the sizes. The local maxima do not coincide with either electronic or atomic shell closing numbers but are bracketed by the two in some cases, suggesting that both effects are relevant to the melting process. Computer simulations have not been able yet to fully explain the experimental results, although Lee et al.<sup>3</sup> have shown that a ratio of the energy contributions of surfacelike and bulklike atoms helps to find some systematics in the melting behavior of clusters of different materials. Experimental results by Schmidt et al.<sup>4</sup> have separated the energetic and entropic contributions to cluster melting and have also found that energetic considerations will play the leading role in an explanation of the size dependence of melting temperatures.

The expectation that melting temperatures of small clusters should be lower than their bulk counterparts is not always true. Jarrold and co-workers have performed ion mobility<sup>5</sup> and multicollision-induced dissociation<sup>6</sup> experiments that demonstrate that small gallium and tin clusters melt at a temperature higher than the corresponding bulk materials. By performing ab initio molecular dynamics simulations, Joshi et al.<sup>7</sup> have shown that  $\text{Sn}_{20}$  shows an enhanced melting temperature because its structure (based on the special stability of a tricapped trigonal prism unit) and bonding nature (covalent) are different from those of bulk tin. Banhart et al.<sup>8</sup> have also observed supercooling and superheating effects in the melting of small tin and lead clusters encapsulated by fullerene-like graphitic shells. In this case, the reason for the superheating is the increased pressure inside the carbon onions.

Yet another interesting feature has been revealed by the experimental work of Schmidt et al.<sup>9</sup> They have shown that negative specific heats may appear in the meltinglike transition of isolated sodium clusters (whose average properties must be calculated according to a microcanonical statistical ensemble). Reyes-Nava et al.<sup>10</sup> have reproduced these negative values in constant-energy molecular dynamics simulations of small Na clusters and have offered an explanation for them in terms of an analysis of kinetic energy distributions and the spread of the distribution of isomers for each size.

Doping a cluster with substitutional impurities introduces new features, which are not present in homogeneous clusters. First, there is the problem of compositional order, which complicates enormously the search for ground-state isomers. Second, surface

\* To whom correspondence may be addressed: E-mail: aguado@metodos.fam.cie.uva.es.

segregation (of the component with lower surface tension) may change the thermal behavior of the cluster in an important way. Third, the introduction of impurity atoms, with different sizes and electronegativities than the host atoms, may change the structure of the host cluster, which will also modify thermal behavior and, in particular, the meltinglike transition. Although most of the work on multicomponent clusters has been devoted to structural properties, a few molecular dynamics simulations exist studying their freezing<sup>11</sup> and melting<sup>12–15</sup> transitions and the influence of temperature on segregation.<sup>16</sup>

Ab initio molecular dynamics methods (aiMD),<sup>17</sup> based on a solution of the Kohn–Sham (KS) equations<sup>18</sup> at each time step, cannot yet be routinely applied to the efficient simulation of dynamical processes in large clusters. Statistical sampling in molecular dynamics simulations can be improved by employing a simplified description of atomic interactions (as exemplified by parametrized interatomic potentials) at the cost of some loss in the accuracy with which interatomic forces are obtained. However, density functional theory (DFT) can provide a better solution to this problem. DFT shows that the total energy of a system of electrons can be expressed in terms of the electronic density,<sup>19</sup> and orbital-free (OF) versions of the aiMD technique have been developed and employed, both in solid state<sup>20–23</sup> and cluster<sup>24–27</sup> applications. OF methods scale linearly with system size, allowing consideration of larger clusters and longer simulation times than typical aiMD simulations, working on a single processor. Although the employment of local pseudopotentials and approximate expressions for the electronic kinetic energy functional reduces the accuracy in the forces acting on the atoms and quantum shell effects are neglected (so that features associated with electronic shell closings are not reproduced), OFMD simulations include an approximate quantum description of the electronic density and provide a more accurate and transferable description of metal clusters than parametrized potentials.

We have used the OFMD method previously to study the meltinglike transition in homogeneous alkali clusters of varying size.<sup>27–30</sup> Our calculated melting temperatures for Na clusters were found to be in very good agreement with the experimental determinations of Haberland's group,<sup>2</sup> which demonstrates the suitability of OF methods to address the problem of cluster melting, at least in the case of the alkalis. The aim of the present work is to employ OFMD simulations to analyze the mechanisms by which the meltinglike transition proceeds in the impurity-doped clusters  $\text{Li}_1\text{Na}_{54}$  and  $\text{Cs}_1\text{Na}_{54}$  and compare their thermal behaviors with those of homogeneous  $\text{Na}_{55}$ .<sup>28</sup> We will show that doping of  $\text{Na}_{55}$  with both impurities results in considerably lower melting temperatures (as determined from peaks in the thermal evolution of the specific heat). We will also analyze the differences in the melting behavior of these clusters, mostly due to the size mismatch between impurity and host atoms. The results of this paper should be considered as the first step of a systematic study of thermal properties of multicomponent clusters, which we are undertaking in our group. In the next section, we briefly present some technical details of the method. The results are presented and discussed in section III, and finally, section IV summarizes our main conclusions.

## II. Theory

In contrast to simulations based on KS single-particle orbitals, OFMD has the electron density as the basic dynamical variable,<sup>19</sup> so an explicit expression for the functional density dependence of the electronic kinetic energy,  $T[n]$ , needs to be introduced. An exact expression for this functional dependence

is not known yet, despite many efforts.<sup>20–22,31,32</sup> The errors associated to the employment of an approximate  $T[n]$  are larger than those associated with approximate exchange-correlation energy functionals, which makes OF less accurate than KS calculations. However, for certain metallic systems such as the alkalis or aluminum, OF methods are sufficiently reliable and much more efficient than KS-based methods, which justifies the employment of OFMD. Our implementation of OFMD is based on an expansion of the electron density in a basis set formed by plane waves. To make this implementation efficient, local pseudopotentials are employed to represent the effect of core electrons on the valence density. Thus, only this valence density is explicitly described. Details of the method have been fully described in our previous work.<sup>27–30</sup> Here we just present briefly the main technical issues.

The electronic kinetic energy functional corresponds to the gradient expansion around the homogeneous limit through the second order<sup>19,33–35</sup>

$$T_s[n] = T^{\text{TF}}[n] + \frac{1}{9} T^{\text{W}}[n] \quad (1)$$

where the first term is the Thomas–Fermi functional

$$T^{\text{TF}}[n] = \frac{3}{10} (3\pi^2)^{2/3} \int n(\vec{r})^{5/3} d\vec{r} \quad (2)$$

and the second is the lowest-order gradient correction, where  $T^{\text{W}}$ , the von Weizsäcker term, is given by

$$T^{\text{W}}[n] = \frac{1}{8} \int \frac{|\nabla n(\vec{r})|^2}{n(\vec{r})} d\vec{r} \quad (3)$$

The local density approximation is used for exchange and correlation.<sup>36,37</sup> In the external field acting on the electrons

$$V_{\text{ext}}(\vec{r}) = \sum_n v(\vec{r} - \vec{R}_n)$$

we take  $v$  to be the local pseudopotential of Fiolhais et al.,<sup>38</sup> which reproduces well the properties of bulk sodium and has been shown to have good transferability to sodium clusters.<sup>39</sup> The suitability of this simple OFMD scheme for the problem at hand will be demonstrated in the next section.

The cluster is placed in a unit cell of a cubic superlattice, and the set of plane waves periodic in the superlattice is used as a basis set to expand the valence density. Present calculations use a supercell with a 35-Å edge and an energy cutoff in the plane-wave expansion of the density of 20 Ryd. A  $96 \times 96 \times 96$  grid is used to perform fast Fourier transforms. The equations of motion are integrated using the velocity Verlet algorithm<sup>40</sup> with a time step equal to 4 (3) fs for temperatures lower (higher) than 100 K. These choices resulted in a conservation of the total energy better than 0.1%. The ground-state electron density is found for each configuration of atoms visited in the course of an MD trajectory, which allows the accurate calculation of atomic forces by means of the Hellmann–Feynman theorem. This is different from our previous implementations of the method,<sup>27</sup> which employed a Car–Parrinello strategy<sup>17</sup> in the MD simulations.

An important first step in the simulation of the meltinglike transition in small clusters is the location of the ground-state isomer. As the number of different isomers is known to increase with size in an exponential way, it is a very hard task to find the minimum energy isomer of a cluster with 55 particles. It is prohibitive, for example, to employ well-behaved methods such

as basin-hopping<sup>41</sup> or genetic algorithms<sup>42</sup> in conjunction with an OF evaluation of cluster energies. Instead, one has to adopt structures that are likely to have the main characteristics of the ground state. In the present case, we have taken complete icosahedral and cuboctahedral structures, as the most plausible candidates, and have considered all possible inequivalent positions for the substitutional impurity. To explicitly check the reliability of OF predictions, we optimize the same structures employing pseudopotential KS-DFT calculations as implemented in SIESTA.<sup>43</sup> This code employs standard norm-conserving pseudopotentials<sup>44</sup> in their fully nonlocal form<sup>45</sup> and a flexible linear combination of atomic orbitals (LCAO) basis set for the description of valence states.<sup>46</sup> The local density approximation is adopted for exchange and correlation effects to be consistent with the reference OF calculations (this way, we test the effect of the approximate kinetic energy functional and local pseudopotential). Standard double- $\zeta$  plus polarization (DZP) basis sets were adopted for each atom. This basis size is found to converge the energies to within 1 meV/atom if the range of the basis functions is carefully optimized. The fineness of the real space grid employed to calculate Hartree and exchange-correlation terms is measured by the maximum kinetic energy of the plane waves that can be represented in the grid without aliasing. A value of 20 Rydbergs is employed, which is also consistent with the OF calculations. In both the OF and SIESTA calculations, we employed a conjugate-gradients technique to obtain optimal geometries for each different isomer.

Starting from an average temperature of 50 K, several molecular dynamics simulation runs at different constant energies were performed in order to obtain the caloric curves. Different values of the average temperature were obtained by isokinetic thermalization runs (approximately 5 ps long) previous to each constant energy run, where the atom velocities are scaled each time step in order to maintain a target temperature. The final configuration of each run served as the starting geometry for the next isokinetic run at a higher temperature. A typical simulation time for the constant energy runs of solidlike clusters is 50 ps, but runs longer than 200 ps were performed for those energies where the melting transition sets in. For energies corresponding to liquidlike clusters, the length of the simulations was always in the range of 70–100 ps. The total simulated time for each cluster was approximately 1.5 ns.

Apart from caloric curves, we have evaluated a number of indicators in order to discuss the details of the meltinglike transition: the specific heat per particle (in units of the Boltzmann constant) defined by<sup>47</sup>

$$C_v = \left[ N - N \left( 1 - \frac{2}{3N-6} \right) \langle E_{\text{kin}} \rangle_t \langle E_{\text{kin}} \rangle_t^{-1} \right]^{-1} \quad (4)$$

where  $N$  is the number of atoms and  $\langle \rangle_t$  indicates the average along a trajectory; the root-mean-square (rms) bond-length fluctuation

$$\delta = \frac{2}{N(N-1)} \sum_{i < j} \frac{(\langle R_{ij}^2 \rangle_t - \langle R_{ij} \rangle_t^2)^{1/2}}{\langle R_{ij} \rangle_t} \quad (5)$$

where  $R_{ij}$  is the distance between atoms  $i$  and  $j$ . By restricting the sum to specific pairs of atoms, one can also evaluate separate fluctuations for Na–Na, Li–Na, and Cs–Na bond lengths; the diffusion coefficient of atoms of species A

$$D_A = \frac{1}{6} \frac{d}{dt} \langle r_A^2(t) \rangle \quad (6)$$

which is obtained from the long time behavior of the corresponding mean-square displacement

$$\langle r_A^2(t) \rangle = \frac{1}{N_A n_t} \sum_{j=1}^{n_t} \sum_{i=1}^{N_A} [\vec{R}_i(t_{0j} + t) - \vec{R}_i(t_{0j})]^2$$

, where  $n_t$  is the number of time origins,  $t_{0j}$ , considered along a trajectory and  $N_A$  is the number of atoms of species A; short-time averages of the “atomic equivalence indexes”,<sup>48</sup> defined for each atom by

$$\sigma_i(t) = \sum_j |\vec{R}_i(t) - \vec{R}_j(t)| \quad (7)$$

the average over a whole dynamical trajectory of the radial atomic distribution function  $g(r)$ , defined by

$$dN_{\text{at}}(r) = g(r) dr \quad (8)$$

where  $dN_{\text{at}}(r)$  is the number of atoms at distances from the center of mass between  $r$  and  $r + dr$ , and finally, to analyze variations in the global shape of the cluster, we have evaluated the rms radius of the cluster  $r$ , a shape deformation parameter  $\beta$  measuring the degree of asphericity, and another parameter  $\gamma$  quantifying its triaxiality. Following Bulgac and Kusnezov,<sup>49</sup> these parameters may be obtained from the three principal moments of inertia (with all the atoms assumed to have the same mass,  $m = 1$  amu),  $I_1 \geq I_2 \geq I_3$ , as follows

$$I_k = \frac{2}{3} r^2 \left( 1 + \beta \sin \left( \gamma + \frac{(4k-3)\pi}{6} \right) \right) \quad (9)$$

$$I_1 + I_2 + I_3 = 2r^2 \quad (10)$$

$\gamma = 0$  corresponds to an axially symmetric prolate aggregate (cigarlike), while for  $\gamma = \pi/3$ , we have an oblate axially symmetric shape (pancake). For intermediate  $\gamma$  values, cluster deformation is triaxial. If  $\beta = 0$ , the shape is spherical and the  $\gamma$  parameter has not any meaning. If  $\gamma = \pi/3$ , the maximum value of  $\beta$  is 0.5, corresponding to a disk of zero thickness. If  $\gamma = 0$ , the maximum value of  $\beta$  is 1, corresponding to a linear chain.

### III. Results

**A. Lowest-Energy Isomers.** An impurity atom may be allocated in four inequivalent positions of a host Na<sub>55</sub> icosahedron: (a) at the center of the icosahedron, (b) at any of the 12 equivalent positions within the first icosahedral shell, (c) at a vertex position of the second icosahedral shell (again, the multiplicity of this site is 12), and (d) at any of the 30 nonvertex sites of the outer shell. We have considered all four possibilities, starting from a perfect icosahedral structure and relaxing the positions of the atoms until the force on each atom is smaller than 0.001 eV/Å. In Table 1, we show OF and SIESTA results for the relative stabilities of these isomers. For the cuboctahedral isomers, we only show in Table 1 the energies of an isomer with the impurity in an inner position (isomer e) and another with the impurity located at a surface site (isomer f). A schematic view of all these isomers may be seen in Figure 1. SIESTA results demonstrate that icosahedral isomers are more stable than corresponding cuboctahedral isomers. Also, as expected from surface energy arguments, the Li atom gets trapped in the central position of the icosahedral host, while the bigger Cs atom prefers the outermost vertex site. A very



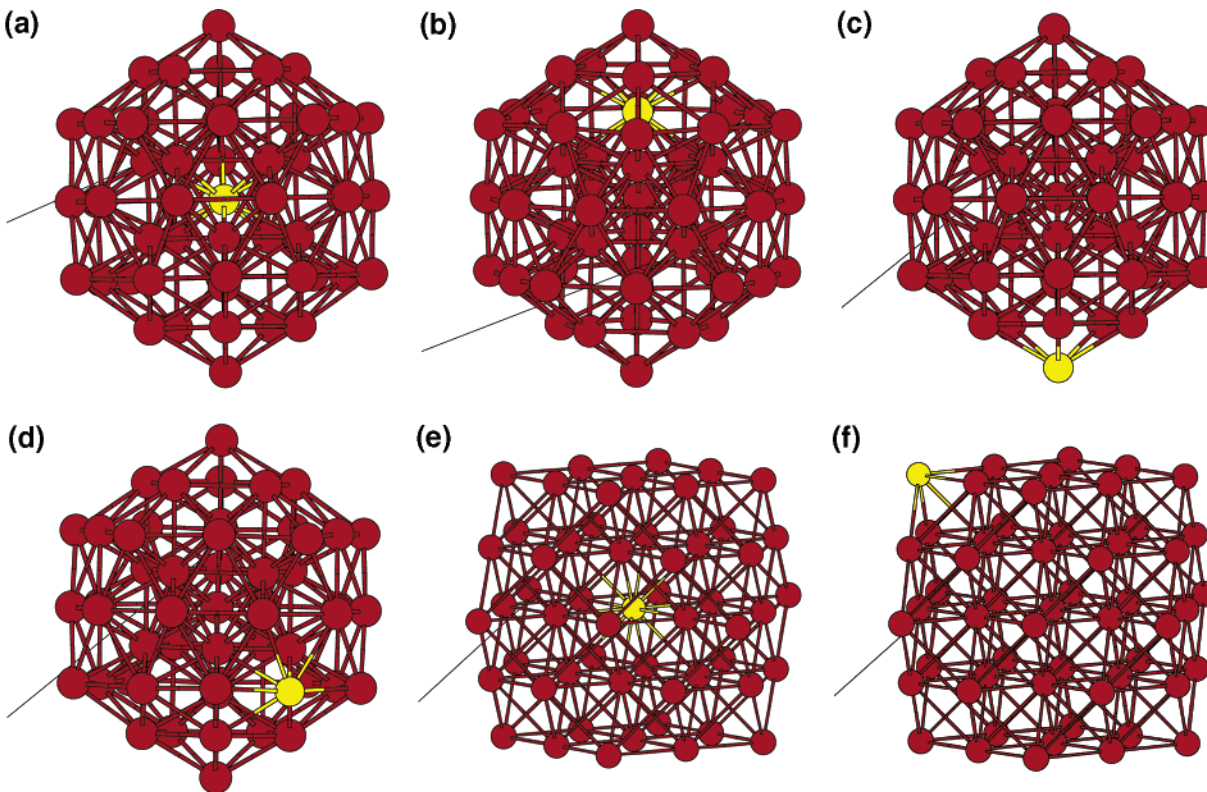


**Figure 1.** Lowest-energy structure and low-lying icosahedral and cuboctahedral isomers considered in this work. Dark balls represent Na atoms, and light balls represent impurity atoms (either Li or Cs). Isomers a to f are as described in the caption to Table 1.

**TABLE 1: Energies (in meV/atom) of Several Isomers of  $\text{Li}_1\text{Na}_{54}$  and  $\text{Cs}_1\text{Na}_{54}$  Clusters, Taking the Energy of the Corresponding Ground State (GS) Isomer as a Reference<sup>a</sup>**

	a	b	c	d	e	f
$\text{Li}_1\text{Na}_{54}$						
SIESTA	GS	2.3	5.6	5.2	10.5	19.1
OF	GS	2.6	5.3	5.0	11.8	18.8
$\text{Cs}_1\text{Na}_{54}$						
SIESTA	10.0	9.6	GS	1.1	15.1	13.7
OF	11.1	10.0	GS	1.5	17.0	14.4

<sup>a</sup> Isomers a to d are icosahedral, as discussed in the text. Isomers e and f are cuboctahedral with the impurity atom located at the center of the cuboctahedron (e) or at a surface position (f).

important observation is that OF calculations reproduce SIESTA results for the relative stabilities of these isomers with a high accuracy, which shows the adopted OF procedure is reliable. We have also analyzed the distributions of interatomic distances obtained from both procedures. The detailed structural distortions induced by the impurities are qualitatively the same in both methods, and the only difference is that all OF distances are systematically longer by approximately 1%, an error which is well within the expected transferability limitations of the employed local pseudopotentials.<sup>39</sup>

The ground-state  $\text{Li}_1\text{Na}_{54}$  isomer predicted by SIESTA is not perfectly icosahedral but shows a small oblate distortion ( $I_1 > I_2 = I_3$ ). A similar prediction has been done in the past for the homogeneous  $\text{Na}_{55}^+$  cluster by Kümmel et al.<sup>50</sup> These authors have shown that oblate distortions lead to a much better agreement between calculated and experimental photoabsorption spectra than that obtained with prolate distortions (which are predicted by jelliumlike models). What is remarkable in our case is that OF calculations also reproduce this slight oblate distortion, a distortion which is maintained at finite temperatures approaching the melting transition (see next section).

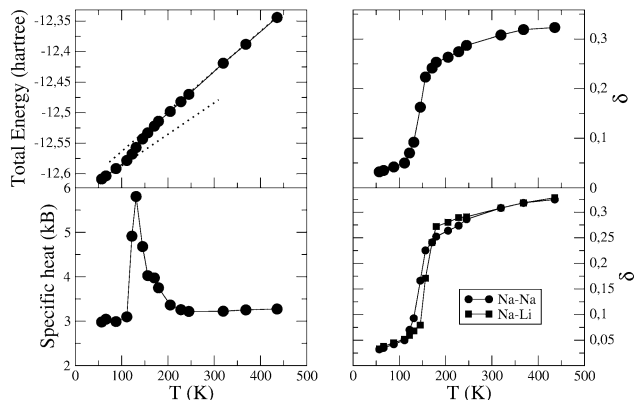


**Figure 2.** Caloric and specific heat curves (left side) and total and partial rms bond-length fluctuations (right side) of  $\text{Li}_1\text{Na}_{54}$ , taking the internal cluster temperature as the independent variable. Prolongation of the solid and liquid branches of the caloric curve is shown by dotted lines, which are employed to estimate the latent heat of fusion.

**B. Meltinglike Transition in  $\text{Li}_1\text{Na}_{54}$ .** In Figure 2, we show the caloric curve, specific heat, and total and partial rms bond-length fluctuations of  $\text{Li}_1\text{Na}_{54}$ , as a function of average temperature. A thermal phase transition is indicated in the caloric curve by a change of slope, the slope being the specific heat; the height of the step gives an estimate of the latent heat of fusion. However, melting processes are more easily recognized as peaks in the specific heat or steps in  $\delta$ , as a function of temperature. All three indicators lead to the same value for the estimated melting temperature (approximately 130 K), which is a good check for the convergence of our results. Our estimation for the latent heat of fusion is about 0.5 eV.

Apart from the main peak, the specific heat displays a shoulder or incipient peak at approximately 160 K, which suggests a stepwise melting process that we analyze in the following. The atomic equivalence indexes, shown in Figure 3,

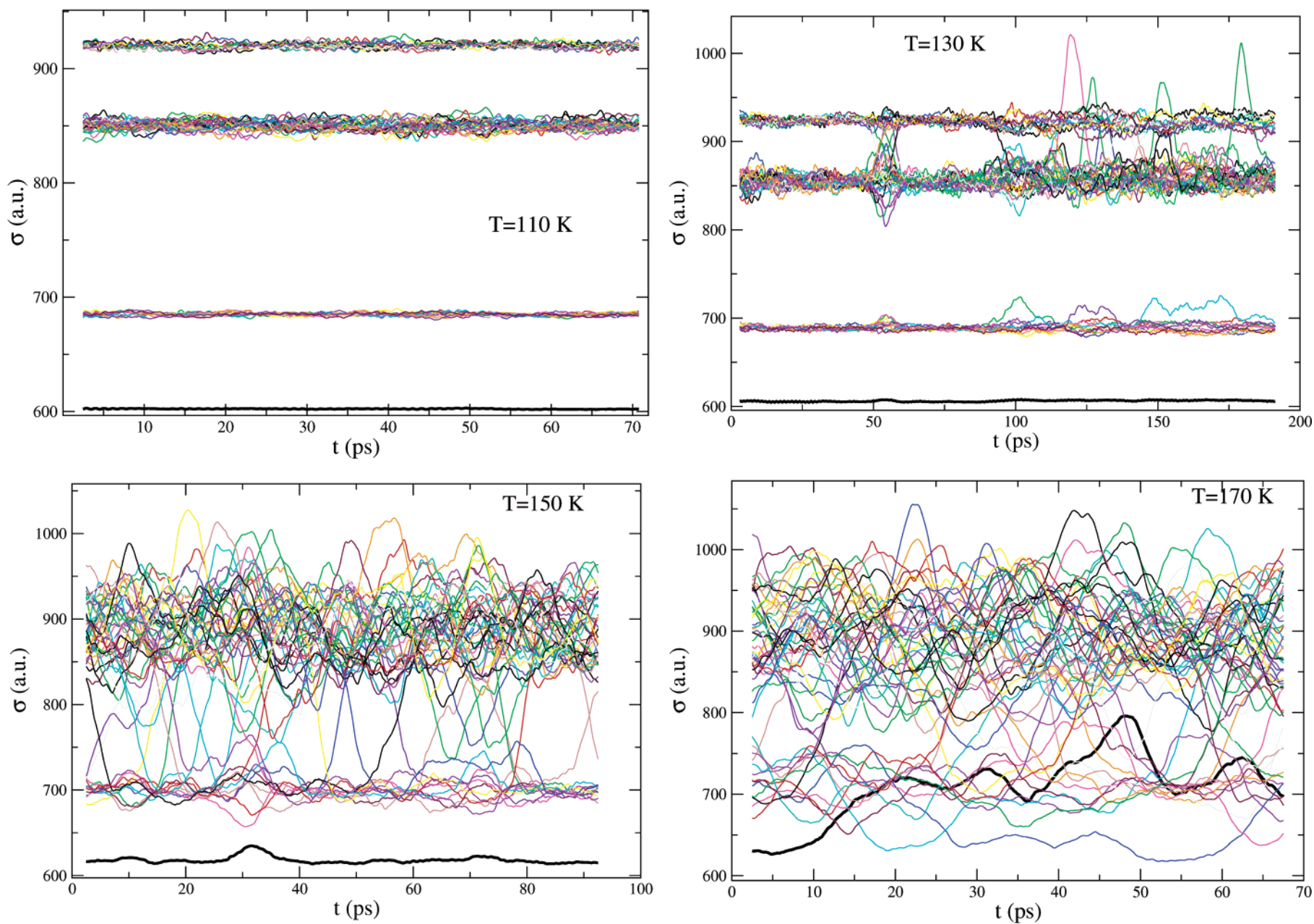


**Figure 3.** Time evolution of atomic equivalence indexes of  $\text{Li}_1\text{Na}_{54}$ , averaged over 1000 time steps, for representative temperature values. The  $\sigma$  curve corresponding to the Li impurity is represented by a bold line.

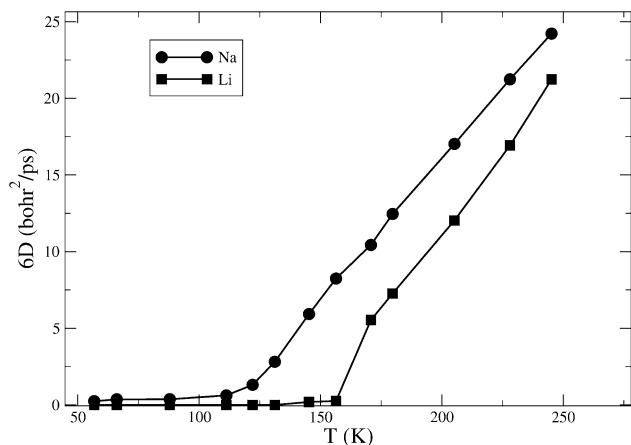


**Figure 4.** Temperature dependence of diffusion coefficients of Li<sub>1</sub>-Na<sub>54</sub>.

are the indicators that provide the most detailed picture of melting, of all those introduced in the previous section. For a solidlike cluster,  $\sigma_i$  takes a different value for each geometrically inequivalent atom in the cluster. For a 55-atom icosahedron, we have four inequivalent sets, as discussed above. When melting or isomerization transitions set in, interchange of atoms between these sets will be observed (if the transition involves only interchanges between symmetry-equivalent atoms, it may still be possible to observe it in the time evolution of  $\sigma_i$ , because transition-state atomic configurations are visited, which usually have a different set of  $\sigma$  values). Figure 3 shows that the cluster begins to melt at 130 K, but the surface and inner radial shells of atoms do not mix yet, at least within the time scale of our simulation (200 ps). Visualization of MD movies shows that the cluster surface melts first. The interchange of atomic positions at the surface involves large outward motions of some surface atoms (Figure 3b), which in turn facilitate large atomic displacements in the inner icosahedral shell. This “intrashell” melting temperature is in correspondence with the main specific heat peak and also with the step in  $\delta$  (see Figure 2). At  $T \approx 145$  K (Figure 3c), mixing of surface and inner Na layers is possible, but the Li atom still remains in its central position. This is in line with the steplike increase in the Li–Na bond-length fluctuation (Figure 2), as some Na atoms initially in the first icosahedral shell (and thus “bonded” to the lithium atom) escape now to the surface. In Figure 4, we show the temperature evolution of the diffusion constants, which shows  $D_{\text{Li}}$  is still close to zero at 145 K, while  $D_{\text{Na}}$  already takes substantially larger values. Finally, at  $T \approx 160$  K (Figure 3d), the Li atom moves out of its central position and begins to diffuse, although only interchanges with interior Na atoms are observed, that is, Li tries to avoid the cluster surface.

This stepwise melting behavior is difficult to observe in the specific heat, as the height of the shoulder observed at approximately 160 K is well within the expected statistical error for  $C_V$  at that temperature. This is because the specific heat is a more global quantity, measuring the increase in available phase space with increasing temperature. Thus, if we were to strictly consider that a cluster is in a liquidlike phase only when all atoms are diffusing across the whole cluster volume (this definition makes sense only if the components of the mixture are miscible in the liquid phase), we should not associate the main peak in the specific heat with the solid–liquid transition temperature but just with the critical temperature at which the largest increase in available phase space occurs. In fact, the Li atom begins to diffuse across the whole cluster volume (including the surface) only when a temperature of 210 K is

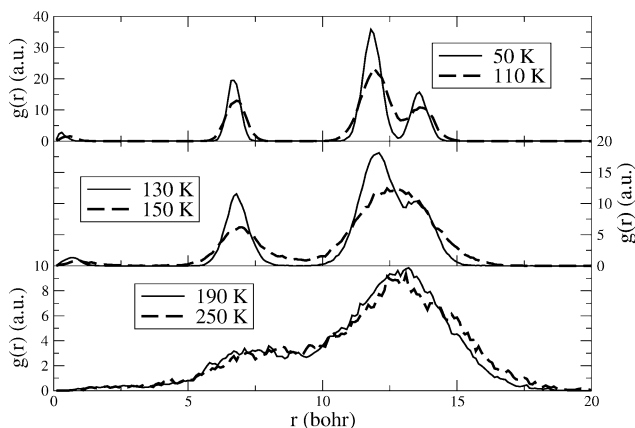


**Figure 5.** Time-averaged radial atomic density distributions of Li<sub>1</sub>-Na<sub>54</sub>, at some representative temperatures.

reached. This temperature is indeed higher than the melting temperature of Na<sub>55</sub>, equal to 190 K<sup>28</sup> (both criteria give the same result in the case of Na<sub>55</sub>).

In a liquidlike cluster, we also expect the radial atomic density distribution to become parabolic (which means that radial order has been washed out in the thermal average), with a long-range decreasing tail due to the diffuse cluster surface. The temperature evolution of  $g(r)$  is shown in Figure 5. At the lowest temperature,  $T = 50$  K, atoms are distributed in two well-separated shells (surface and inner shells) and the central atom; two different subshells form in the surface shell, corresponding to atoms in vertex (surface coordination equal to 5) and nonvertex (surface coordination equal to 6) positions. With increasing temperature, the distribution of atoms is more and more homogeneous and individual peaks merge into one single peak. However, at a temperature as high as 250 K, the distribution is not parabolic yet, showing that the probability (per unit area) of finding an atom in a given infinitesimal radial shell

$$\left( \frac{g(r) dr}{4\pi r^2} \right)$$

is not constant, which means some radial order still remains. If we define the liquid state as that leading to a strictly homogeneous average distribution of atoms, the cluster would be completely liquid only at 280 K.

It is interesting here to compare the distribution of atoms for our simulated liquid cluster with that found at the surface of bulk liquid Na. González et al.<sup>51</sup> have performed OFMD simulations for a slab of 2000 Na atoms. Their atomic density profiles show a pronounced stratification extending several atomic diameters into the bulk, a behavior previously observed in other metals.<sup>52</sup> There are several tentative explanations for the observed layering: Rice and co-workers<sup>53</sup> suggest that the abrupt decay of the electron density at the surface provides an effective potential wall for the atoms, against which they stack; Chacón et al.<sup>54</sup> have proposed that the layering is a general property of liquid surfaces at low temperature and is a signature of frustrated crystallization for those materials having a low melting temperature compared to the critical temperature. Our results show that this stratification is also present at the surfaces of small metal liquid clusters and suggest that it is a general feature of finite metal systems. We would like to notice here that, according to experiments by Haberland,<sup>2</sup> the ratio of melting and boiling temperatures is much smaller for sodium clusters ( $T_m/T_b \approx 0.3$ ) than for bulk sodium ( $T_m/T_b \approx 0.6$ ), and yet the surface layering is observed up to relatively high



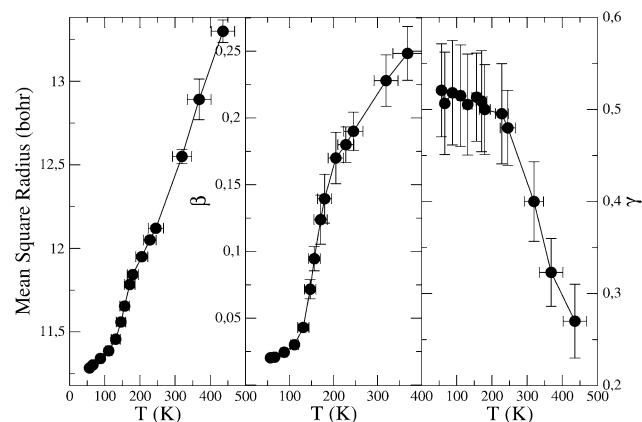


**Figure 6.** Temperature evolution of the mean square radius  $r$  (left), asphericity parameter  $\beta$  (middle), and triaxiality parameter  $\gamma$  (right) of  $\text{Li}_1\text{Na}_{54}$ . Horizontal error bars represent temperature fluctuations (not shown in previous plots); vertical error bars are covariances of cluster shape parameters.

temperatures. We have performed preliminary simulations that show that OFMD-predicted boiling temperatures are of the same order as the experimental ones. Therefore, we are led to conclude that some other factor, apart from a small  $T_m/T_b$  ratio, is needed in order to explain the surface layering in small liquid droplets. More detailed studies will be needed to clarify this issue.

In summary, the specific heat is a very useful indicator of melting because it detects the beginning of the melting transition and is an experimentally accessible quantity,<sup>2</sup> but only an examination of several microscopic indicators can provide us with a complete and consistent picture of the melting process in clusters.

It is also interesting to analyze the temperature dependence of the global cluster shape, as this can be inferred from ion mobility experiments.<sup>5</sup> These results are shown in Figure 6. The mean square radius increases in a pronounced way across the melting transition (by approximately 0.5 au), in line with the expectation that a larger free volume is needed in order to “activate” the liquid state. It is also seen that thermal expansion is larger in the liquid phase, as expected.  $\beta$  is close to zero in the solid phase, which means the cluster is almost spherical. Upon melting, the asphericity degree increases markedly and continues to increase in the liquid phase. The average value of  $\gamma$  clearly decreases with temperature, although its thermal fluctuations are large. Thus, with increasing temperature, the cluster shape is approaching the limit of an axially symmetric prolate cluster. Just before evaporation, the cluster shape is thus predicted to be cigarlike.

**C. Meltinglike Transition in  $\text{Cs}_1\text{Na}_{54}$ .** The results for this cluster are shown in Figures 7–10, in exactly the same way as those for  $\text{Li}_1\text{Na}_{54}$ . The specific heat (Figure 7) shows a broad asymmetric peak with its maximum height at  $T \approx 110$  K. This peak is in correspondence with the slope change in the caloric curve (from which a latent heat of 0.64 eV results) and the stepwise change in the rms bond length fluctuations. In this case, no significant differences between  $\delta_{\text{Na-Na}}$  and  $\delta_{\text{Na-Cs}}$  are observed.

The time evolution of atomic equivalence indexes at 110 K (Figure 8) is indicative of an intrashell melting stage, similar to that found in  $\text{Li}_1\text{Na}_{54}$ . However, a difference is that the impurity atom is now located at the surface. An analysis of the temperature evolution of diffusion coefficients (Figure 9) shows that the Cs atom is not yet moving. Thus, the surface melting is partial and involves only Na atoms, while the Cs impurity remains in its vertex position at the surface. This is most

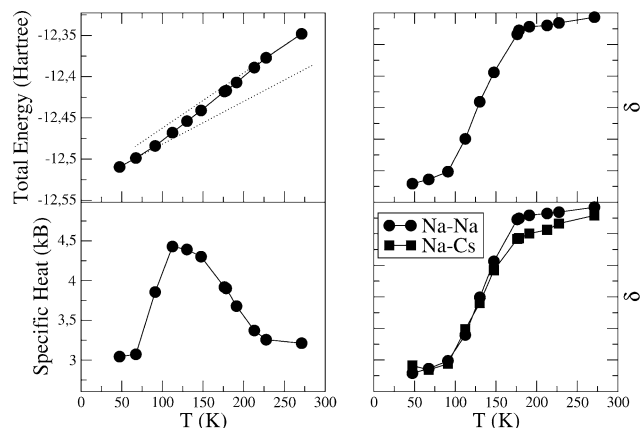


**Figure 7.** Caloric and specific heat curves (left side) and total and partial rms bond length fluctuations (right side) of  $\text{Cs}_1\text{Na}_{54}$ , taking the internal cluster temperature as the independent variable. To better appreciate the transition, the highest temperatures are not explicitly shown. Prolongation of the solid and liquid branches of the caloric curve are shown by dotted lines, which are employed to estimate the latent heat of fusion.

probably due to the large size of Cs enhancing the barriers against Cs diffusion in a Na matrix. Only when outer and inner atomic shells mix ( $T \approx 130$  K) is the Cs atom able to participate in diffusion (Figure 9). Nevertheless, movement of the Cs atom is restricted to the cluster surface. Again, the large size of the Cs atom inhibits its insertion inside the cluster. Surface segregation of the Cs atom is maintained up to the highest temperature considered (450 K). Regarding the radial distribution of atoms within the cluster, it becomes strictly homogeneous only at  $T \approx 300$  K.

The temperature evolution of cluster shape parameters is shown in Figure 10. Both the mean square radius and asphericity increase markedly upon melting, the same behavior found for  $\text{Li}_1\text{Na}_{54}$ . However, the triaxiality parameter  $\gamma$  does not decrease with temperature in a pronounced way. As Cs is much heavier than Na, it tends to favor oblate shape distortions, as it prefers to be located along the axis with the largest moment of inertia. This tendency seems to be in competition with the general preference toward prolate distortions at high temperatures found in  $\text{Li}_1\text{Na}_{54}$  and pure Na clusters.<sup>27</sup> We cannot conclude from an analysis of Figure 10 whether an oblate or prolate shape will prevail at higher temperatures.

#### IV. Summary and Discussion

In this paper, an efficient OF molecular dynamics method has been employed to study the meltinglike transitions of  $\text{Li}_1\text{Na}_{54}$  and  $\text{Cs}_1\text{Na}_{54}$ . The accuracy of the proposed scheme has been demonstrated by direct comparison to ab initio KS calculations. Our calculations predict icosahedral structures to be more stable than cuboctahedral structures for both clusters. Lowest-energy isomers are found with the Li impurity located at the center of the icosahedron and the Cs impurity located at a vertex surface position.

The meltinglike transition proceeds stepwise in both cases, although the thermal evolution of the specific heat presents just one broad peak. Thus, we have analyzed a variety of melting indicators in order to obtain a complete picture of the melting mechanism. In a first stage, the two icosahedral shells melt separately but radial order is maintained, that is, no mixing of atoms in different radial shells is observed. Also, in this first melting stage, impurity atoms do not participate in diffusion. As temperature increases, mixing of inner and surface shells

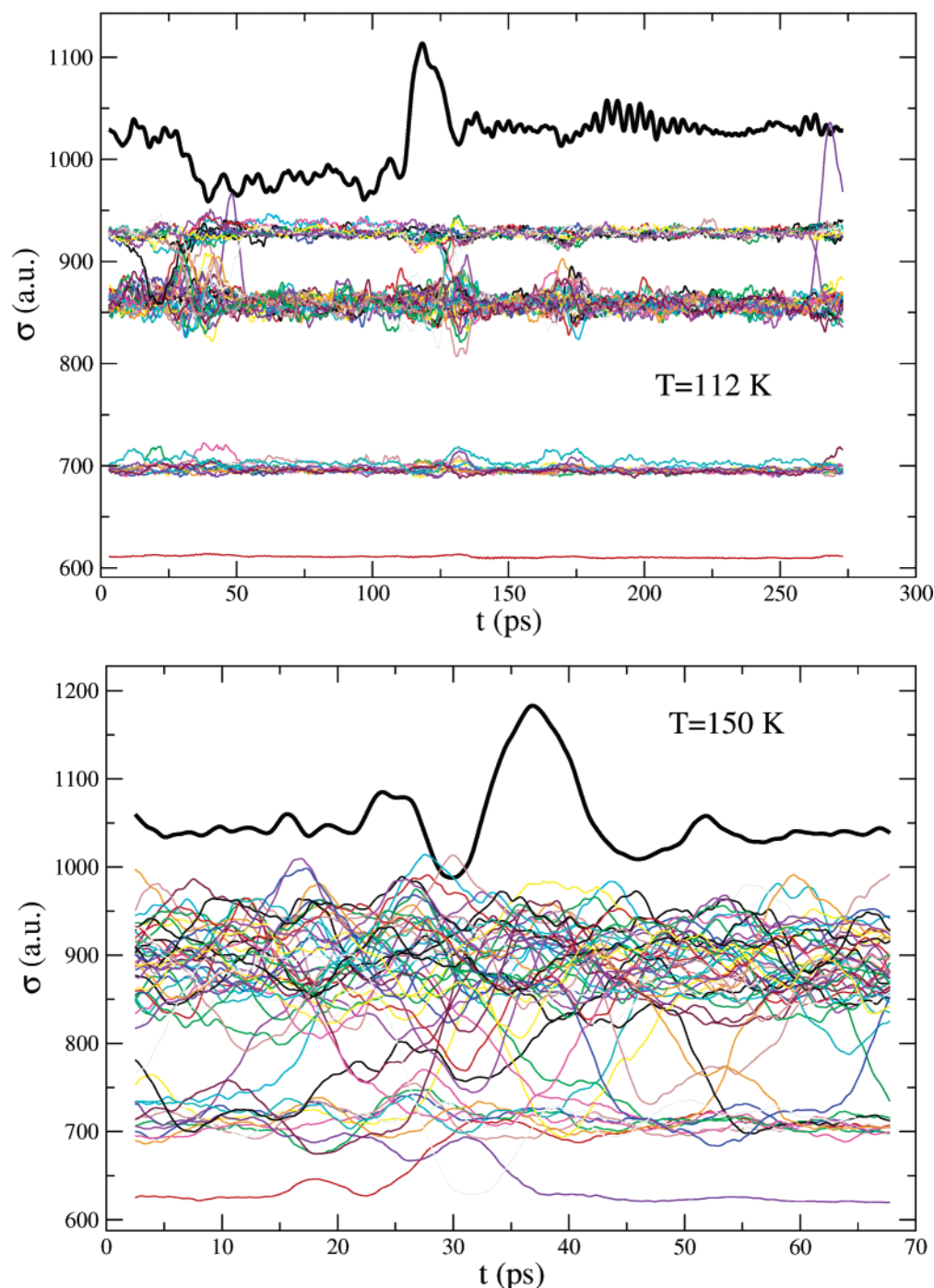


**Figure 8.** Time evolution of atomic equivalence indexes of  $\text{Cs}_1\text{Na}_{54}$ , averaged over 1000 time steps, for representative temperature values. The  $\sigma$  curve corresponding to the Cs impurity is represented by a bold line.

progressively increases and impurity atoms begin to participate in diffusion events. The Li impurity is found to visit the cluster surface environment for sufficiently high temperatures. A Cs impurity, on the contrary, remains on the surface for the whole range of temperatures considered. The shape of both clusters becomes aspherical upon melting, with the asphericity degree increasing with temperature. Close to the evaporation limit,  $\text{Li}_1\text{Na}_{54}$  is predicted to be cigarlike (prolate distortion), while it is not clear if  $\text{Cs}_1\text{Na}_{54}$  will adopt a prolate or an oblate shape.

Meltinglike transitions in clusters are usually detected by examining the thermal evolution of the specific heat. This is a very important indicator as it can be experimentally determined.<sup>2</sup> However, being a thermal (as opposed to structural) indicator, it does not provide enough information about the mechanisms

by which melting proceeds. In this paper, we have shown that the specific heat peak locates the beginning of the meltinglike transition for  $\text{Li}_1\text{Na}_{54}$  and  $\text{Cs}_1\text{Na}_{54}$ . However, at a temperature corresponding to the main peak in the specific heat, those clusters cannot be considered to be fully liquid, because not all the atoms in the cluster are diffusing. Diffusion constants are thus proposed as more useful indicators to decide at which temperature is a cluster to be considered fully fluid. We have also proposed the employment of the average radial distribution of atoms as an indicator of the liquid state in clusters. Specifically, we consider that a cluster is fully liquid when the average distribution of atoms is completely homogeneous. This is proposed as a useful indicator to locate the end of the melting transition.



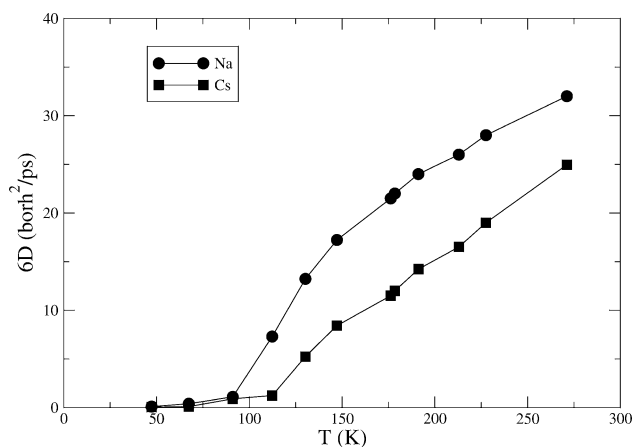


**Figure 9.** Temperature dependence of diffusion coefficients of Cs<sub>1</sub>-Na<sub>54</sub>.

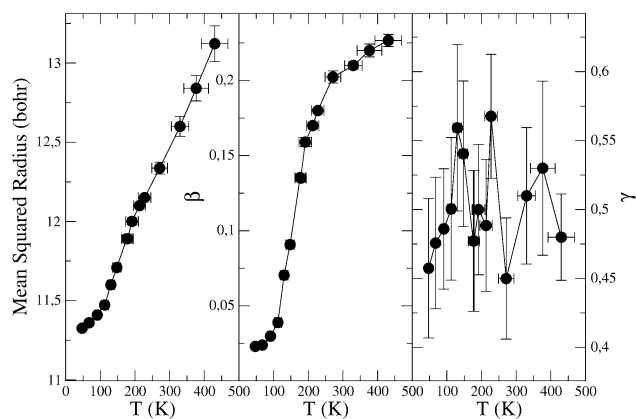


**Figure 10.** Temperature evolution of the mean square radius  $r$  (left), asphericity parameter  $\beta$  (middle), and triaxiality parameter  $\gamma$  (right) of Cs<sub>1</sub>Na<sub>54</sub>. Horizontal error bars represent temperature fluctuations (not shown in previous plots); vertical error bars are covariances of cluster shape parameters.

Doping of Na<sub>55</sub> with both Li and Cs is found to significantly lower its melting temperature (as determined from the main peak in the specific heat). This is in line with bulk melting behavior, where it is known that defects in the crystalline lattice (and substitutional impurities are just a specific kind of defect) provide nucleation sites for the liquid phase. However, this should not be considered a completely general result, as some specific impurities (for example, those which lead to a local change from metallic to a stronger ionic bonding) may be expected to enlarge the stability limit of the solid phase, even if they also represent a defect in the host lattice. In these cases, doping may lead to phase separation (the metallic part of the host cluster melts at a low temperature, while the ionic-like part close to the impurity remains solid up to higher temperatures). At the same time, the average distribution of atoms for the doped clusters becomes homogeneous at much higher temperatures than those of pure Na<sub>55</sub>, which shows the meltinglike transition proceeds in a wider temperature range upon doping. Regarding the melting mechanism, stepwise melting has been observed in simulations of some alkali clusters.<sup>27–30</sup> This is due to the appearance of a surface melting stage prior to homogeneous melting in large alkali clusters and to isomerization premelting effects in small Na clusters. In impurity-doped clusters as those considered here, impurity atoms begin to participate in diffusion events at different temperatures than host (Na) atoms, which provides another mechanism for stepwise melting in multicomponent clusters, not present in one-component clusters. We will

leave further investigations on melting of multicomponent clusters of different concentrations (nanoalloys) to future studies.

**Acknowledgment.** This work was supported by Junta de Castilla y León (Project VA073/02) and DGES (Project MAT2002-04393-C02-01). Thanks are due to J. M. Soler and his team for providing us with a copy of the SIESTA code. A. Aguado also acknowledges financial support from the Spanish Ministry of Science and Technology, under the Ramón y Cajal program.

## References and Notes

- (1) Wang, Z. L.; Petroski, J. M.; Green, T. C.; El-Sayed, M. A. *J. Phys. Chem. B* **1998**, *102*, 6145.
- (2) (a) Schmidt, M.; Kusche, R.; Kronmüller, W.; von Issendorff, B.; Haberland, H. *Phys. Rev. Lett.* **1997**, *79*, 99. (b) Schmidt, M.; Kusche, R.; von Issendorff, B.; Haberland, H. *Nature* **1998**, *393*, 238. (c) Kusche, R.; Hippler, Th.; Schmidt, M.; von Issendorff, B.; Haberland, H. *Eur. Phys. J. D* **1999**, *9*, 1. (d) Schmidt, M.; Haberland, H. *C. R. Phys.* **2002**, *3*, 327.
- (3) Lee, Y. J.; Lee, E. K.; Kim, S.; Nieminen, R. M. *Phys. Rev. Lett.* **2001**, *86*, 999.
- (4) Schmidt, M.; Donges, J.; Hippler, Th.; Haberland, H. *Phys. Rev. Lett.* **2003**, *90*, 103401.
- (5) Shvartsburg, A. A.; Jarrold, M. F. *Phys. Rev. Lett.* **2000**, *85*, 2530.
- (6) Breaux, G. A.; Benirschke, R. C.; Sugai, T.; Kinnear, B. S.; Jarrold, M. F. *Phys. Rev. Lett.* **2003**, *91*, 215508.
- (7) Joshi, K.; Kanhere, D. G.; Blundell, S. *Phys. Rev. B* **2003**, *67*, 235413.
- (8) Banhart, F.; Hernández, E.; Terrones, M. *Phys. Rev. Lett.* **2003**, *90*, 185502.
- (9) Schmidt, M.; Kusche, R.; Hippler, T.; Donges, J.; Kronmüller, W.; von Issendorff, B.; Haberland, H. *Phys. Rev. Lett.* **2001**, *86*, 1191.
- (10) Reyes-Nava, J. A.; Garzón, I. L.; Michaelian, K. *Phys. Rev. B* **2003**, *67*, 165401.
- (11) Chushak, Y. G.; Bartell, L. S. *J. Phys. Chem. B* **2003**, *107*, 3747.
- (12) López, M. J.; Marcos, P. A.; Alonso, J. A. *J. Chem. Phys.* **1996**, *104*, 1056.
- (13) Huang, S.; Balbuena, P. P. *J. Phys. Chem. B* **2002**, *106*, 7225.
- (14) Joshi, K.; Kanhere, D. G. *Phys. Rev. A* **2002**, *65*, 043203.
- (15) Joshi, K.; Kanhere, D. G. *J. Chem. Phys.* **2003**, *119*, 12301.
- (16) Mainardi, D. S.; Balbuena, P. P. *Int. J. Quantum Chem.* **2001**, *85*, 580.
- (17) (a) Car, R.; Parrinello, M. *Phys. Rev. Lett.* **1985**, *55*, 2471. (b) Payne, M. C.; Teter, M. P.; Allan, D. C.; Arias, T. A.; Joannopoulos, J. D. *Rev. Mod. Phys.* **1992**, *64*, 1045.
- (18) Kohn, W.; Sham, L. J. *Phys. Rev.* **1965**, *140*, 1133A.
- (19) Hohenberg, P.; Kohn, W. *Phys. Rev.* **1964**, *136*, 864B.
- (20) (a) Chacón, E.; Alvarellos, J. E.; Tarazona, P. *Phys. Rev. B* **1985**, *32*, 7868. (b) García-González, P.; Alvarellos, J. E.; Chacón, E. *Phys. Rev. B* **1996**, *53*, 9509. (c) García-González, P.; Alvarellos, J. E.; Chacón, E. *Phys. Rev. A* **1996**, *54*, 1897. (d) García-González, P.; Alvarellos, J. E.; Chacón, E. *Phys. Rev. B* **1998**, *57*, 4857. (e) García-González, P.; Alvarellos, J. E.; Chacón, E. *Phys. Rev. A* **1998**, *57*, 4192.
- (21) (a) Pearson, M.; Smargiassi, E.; Madden, P. A. *J. Phys.: Condens. Matter* **1993**, *5*, 3221. (b) Smargiassi, E.; Madden, P. A. *Phys. Rev. B* **1994**, *49*, 5220. (c) Foley, M.; Smargiassi, E.; Madden, P. A. *J. Phys.: Condens. Matter* **1994**, *6*, 5231. (d) Smargiassi, E.; Madden, P. A. *Phys. Rev. B* **1995**, *51*, 117. (e) Smargiassi, E.; Madden, P. A. *Phys. Rev. B* **1995**, *51*, 129. (f) Foley, M.; Madden, P. A. *Phys. Rev. B* **1996**, *53*, 10589. (g) Jesson, B. J.; Foley, M.; Madden, P. A. *Phys. Rev. B* **1997**, *55*, 4941. (h) Anta, J. A.; Jesson, B. J.; Madden, P. A. *Phys. Rev. B* **1998**, *58*, 6124.
- (22) (a) Govind, N.; Wang, Y. A.; Carter, E. A. *J. Chem. Phys.* **1999**, *110*, 7677. (b) Wang, Y. A.; Govind, N.; Carter, E. A. *Phys. Rev. B* **1999**, *60*, 16350. (c) Watson, S. C.; Carter, E. A. *Comput. Phys. Comm.* **2000**, *128*, 67.
- (23) González, D. J.; González, L. E.; López, J. M.; Stott, M. J. *J. Chem. Phys.* **2001**, *115*, 2373.
- (24) (a) Shah, V.; Nehete, D.; Kanhere, D. G. *J. Phys.: Condens. Matter* **1994**, *6*, 10773. (b) Nehete, D.; Shah, V.; Kanhere, D. G. *Phys. Rev. B* **1996**, *53*, 2126. (c) Shah, V.; Kanhere, D. G. *J. Phys.: Condens. Matter* **1996**, *8*, L253. (d) Shah, V.; Kanhere, D. G.; Majumder, C.; Das, G. P. *J. Phys.: Condens. Matter* **1997**, *9*, 2165. (e) Vichare, A.; Kanhere, D. G. *J. Phys.: Condens. Matter* **1998**, *10*, 3309. (f) Vichare, A.; Kanhere, D. G. *Eur. Phys. J. D* **1998**, *4*, 89. (g) Dhavale, A.; Shah, V.; Kanhere, D. G. *Phys. Rev. A* **1998**, *57*, 4522.
- (25) (a) Govind, N.; Mozos, J. L.; Guo, H. *Phys. Rev. B* **1995**, *51*, 7101. (b) Wang, Y. A.; Govind, N.; Carter, E. A. *Phys. Rev. B* **1998**, *58*, 13465.
- (26) Blaise, P.; Blundell, S. A.; Guet, C. *Phys. Rev. B* **1997**, *55*, 15856.

- (27) Aguado, A.; López, J. M.; Alonso, J. A.; Stott, M. J. *J. Chem. Phys.* **1999**, *111*, 6026.
- (28) Aguado, A.; López, J. M.; Alonso, J. A.; Stott, M. J. *J. Phys. Chem. B* **2001**, *105*, 2386.
- (29) Aguado, A.; Molina, L. M.; López, J. M.; Alonso, J. A. *Eur. Phys. J. D* **2001**, *15*, 221.
- (30) Aguado, A. *Phys. Rev. B* **2001**, *63*, 115404.
- (31) Karasiev, V. V.; Ludeña, E. V.; Artemyer, A. N. *Phys. Rev. A* **2000**, *62*, 062510.
- (32) Wang, B.; Stott, M. J.; von Barth, U. *Phys. Rev. A* **2001**, *63*, 052501.
- (33) *Theory of the inhomogeneous electron gas*; Lundqvist, S., March, N. H., Eds.; Plenum Press: New York, 1983.
- (34) Yang, W. *Phys. Rev. A* **1986**, *34*, 4575.
- (35) Perdew, J. P. *Phys. Lett. A* **1992**, *165*, 79.
- (36) Perdew, J. P.; Zunger, A. *Phys. Rev. B* **1981**, *23*, 5048.
- (37) Ceperley, D.; Alder, B. *Phys. Rev. Lett.* **1980**, *45*, 566.
- (38) (a) Fiolhais, C.; Perdew, J. P.; Armster, S. Q.; McLaren, J. M.; Brajczewska, H. *Phys. Rev. B* **1995**, *51*, 14001. (b) Fiolhais, C.; Perdew, J. P.; Armster, S. Q.; McLaren, J. M.; Brajczewska, H. *Phys. Rev. B* **1996**, *53*, 13193.
- (39) Nogueira, F.; Fiolhais, C.; He, J.; Perdew, J. P.; Rubio, A. *J. Phys.: Condens. Matter* **1996**, *8*, 287.
- (40) (a) Verlet, L. *Phys. Rev.* **1967**, *159*, 98. (b) Swope, W. C.; Andersen, H. C. *J. Chem. Phys.* **1982**, *76*, 637.
- (41) Wales, D. J.; Scheraga, H. A. *Science* **1999**, *285*, 1368.
- (42) Johnston, R. L. *Dalton Trans.* **2003**, *22*, 4193.
- (43) Soler, J. M.; Artacho, E.; Gale, J. D.; García, A.; Junquera, J.; Ordejón, P.; Sánchez-Portal, D. *J. Phys.: Condens. Matter* **2002**, *14*, 2475.
- (44) Hamann, D. R.; Schlüter, M.; Chiang, C. *Phys. Rev. Lett.* **1979**, *43*, 1494.
- (45) Kleinman, L.; Bylander, D. M. *Phys. Rev. Lett.* **1982**, *48*, 1425.
- (46) Anglada, E.; Soler, J. M.; Junquera, J.; Artacho, E. *Phys. Rev. B* **2002**, *66*, 205101.
- (47) Sugano, S. *Microcluster Physics*; Springer-Verlag: Berlin, 1991.
- (48) (a) Bonacić-Koutecký, V.; Jellinek, J.; Wiechert, M.; Fantucci, P. *J. Chem. Phys.* **1997**, *107*, 6321. (b) Reichardt, D.; Bonacić-Koutecký, V.; Fantucci, P.; Jellinek, J. *Chem. Phys. Lett.* **1997**, *279*, 129.
- (49) Bulgac, A.; Kusnezov, D. *Phys. Rev. B* **1992**, *45*, 1988.
- (50) (a) Kümmel, S.; Brack, M.; Reinhard, P. G. *Phys. Rev. B* **2000**, *62*, 7602. Kümmel, S.; Brack, M.; Reinhard, P. G. *Phys. Rev. B* **2001**, *63*, 129902(E).
- (51) González, D. J.; González, L. E.; Stott, M. J. *Phys. Rev. Lett.* **2004**, *92*, 085501.
- (52) D'Evelyn, M. P.; Rice, S. A. *Phys. Rev. Lett.* **1981**, *47*, 1844.
- (53) Chekmarev, D. S.; Zhao, M.; Rice, S. A. *J. Chem. Phys.* **1998**, *109*, 768.
- (54) Chacón, E.; Reinaldo-Falagán, M.; Velasco, E.; Tarazona, P. *Phys. Rev. Lett.* **2001**, *87*, 166101.